Translational Energy Distributions for Dissociation of the van der Waals Cation Species $(C_6H_6\cdots Ar_n)^+$ (n = 1,2) Measured by Velocity Map Imaging†

Jason R Gascooke and Warren D Lawrance*

School of Chemistry, Physics and Earth Sciences, Flinders University, G.P.O. Box 2100, Adelaide S.A. 5001, Australia

Received: March 29, 2000; In Final Form: June 21, 2000

The kinetic energy distributions associated with ejection of Ar from the cation van der Waals species $(C_6H_6\cdots Ar)^+$ and $(C_6H_6\cdots Ar_2)^+$ have been measured by ion imaging with a velocity mapping configuration. The $(C_6H_6\cdots Ar_2)^+$ dissociation was observed for the isomer with an Ar atom on each side of the benzene ring. The cations were created by (1+1) resonance-enhanced multiphoton ionization via their 6^1_0 transitions. The initial cation vibrational state population distributions were deduced from photoelectron spectra of benzene measured with the velocity map imaging spectrometer. The cations are produced with an average vibrational energy ∼1800−1900 cm^{-1}. For dissociation of $(C_6H_6\cdots Ar_2)^+$, on average enough energy remains in the $(C_6H_6\cdots Ar)^+$ fragment to eject the remaining Ar. The experiment views fragmentation of the subset of the $(C_6H_6\cdots Ar_2)^+$ cations that lose a single Ar and for this reason the initial internal ion energy is significantly lower than 1800 cm^{-1} for the $(C_6H_6\cdots Ar_2)^+$ dissociations monitored. The average initial energies above dissociation are estimated to be ∼1310 and ∼350 cm^{-1} for $(C_6H_6\cdots Ar)^+$ and $(C_6H_6\cdots Ar_2)^+$, respectively. The kinetic energy distributions are well fitted by the function $P(E) = E^{1/2}\{c_1 \exp(-k_1E) + c_2 \exp(-k_2E)\}$. The average kinetic energies released were 92 ± 4 and 78 ± 5 cm^{-1} for $(C_6H_6\cdots Ar)^+$ and $(C_6H_6\cdots Ar_2)^+$, respectively. The lower average kinetic energy released for $(C_6H_6\cdots Ar_2)^+$ is attributed to its lower initial internal energy. For $(C_6H_6\cdots Ar)^+$ the kinetic energy released represents only a small fraction of the total energy that requires redistributing. A large proportion of the total energy is therefore taken up as rotational and vibrational energy of the benzene cation fragment.

1. Introduction

Van der Waals clusters provide a means for the stepwise study of physical properties between a bare molecule and one completely solvated and for this reason there has been extensive study of these species over the past 20 years. A particular feature of van der Waals molecules is their small binding energy. At low energies (and low density of states) it is possible to observe dissociation following preparation of the complex in specific vibrational levels.[1−8] In the case of aromatic−X clusters (X = rare gas, diatomic, or small polyatomic), dispersed fluorescence has usually been used to reveal the final states of the aromatic following cluster dissociation within the excited electronic state. Two color ionization can provide the same information.[9,10] These studies reveal that the dissociation rates depend on the total energy in the cluster, the type of vibration initially excited, and the identity of the cluster partner.

While there have been quite a number of studies of the vibrational energy distributions following van der Waals complex dissociation, few studies have probed the translational energy released. Early work was performed on the ground state benzene dimer $(C_6H_6)_2$, with the recoiling translational energy distribution determined by either time-of-flight methods[11] or from the angular distribution of the fragments.[12] These experiments used an infrared laser to excite either the C−H stretching vibration (∼3000 cm^{-1})[12] or the C−H in plane vibration (∼1000 cm^{-1}).[11,13] Recently, Yoder et al. have used ion imaging to determine the kinetic energy released during dissociation of pyrazine−Ar complexes from the triplet state.[14] Yoder and Barker have used a time-of-flight technique to extend these studies to dissociation of a number of aromatic−X complexes (where X = rare gas and small polyatomic) from the triplet state.[15]

The vast majority of dynamical information on van der Waals complexes containing large polyatomics, for example benzene and substituted benzenes, concerns excited electronic states. There are comparably few measurements concerning the dynamics in the ground electronic state or the corresponding cationic state. Compared with the corresponding closed shell neutral, the cationic clusters have a larger binding energy and are radicals. Ionic clusters might thus be expected to show behavior that differs from that displayed by the neutral.

We here report the results of a study of the kinetic energy released in the dissociation of the cation species $(benzene-Ar_n)^+$ (n = 1, 2). With our present apparatus clusters with n > 2 cannot be studied as they cannot be excited exclusively. The kinetic energy distributions are measured using ion imaging[16,17] with velocity mapping.[18,19] The dissociation occurs from the distribution of initial vibrational levels in the ground electronic state of the cation that are populated by one-color, (1+1) REMPI of the complexes via their 6^1_0 transition. Since one of the products of the dissociation is an atom, the translational energy distribution provides insight into the internal energy remaining in the $(benzene-Ar_{n-1})^+$ fragment.

The process being probed has relevance to the evaporation of energized clusters and to the loss of solvent from a solvent

† Part of the special issue "C. Bradley Moore Festschrift".

* To whom correspondence should be addressed. E-mail address: warren.lawrance@flinders.edu.au. Fax: 61-8-8201 2905.

10.1021/jp0011847 CCC: $19.00
Published on Web 08/19/2000

cage. It also has relevance to collision-induced energy transfer, with van der Waals complex dissociation being described as a "half-collision".[14,15,20,21]

2. Background Information: $C_6H_6\cdots Ar_n$ and $(C_6H_6\cdots Ar_n)^+$

The benzene cation−argon species are produced via REMPI through the $S_1 \leftarrow S_0$ 6^1_0 transitions of the corresponding benzene−argon neutrals. The $S_1 \leftarrow S_0$ transition in benzene is vibronically induced via e_{2g} modes, ν_6 being the most prominent.[22−24]

The $S_1 \leftarrow S_0$ transition of $C_6H_6\cdots Ar$ has been studied extensively. The strong 6^1_0 transition of the complex has been reported to be 21 cm^{-1} red-shifted from the 6^1_0 transition in benzene.[1,25] The rotationally resolved high-resolution spectrum yields the precise value of 21.018 cm^{-1}.[26] The argon atom is located centrally above the benzene ring with an Ar−benzene separation of 3.583 Å in the ground state and 3.523 Å in the excited state.[26] The binding energy was first determined to be >608 cm^{-1} in the ground state and >629 cm^{-1} in the excited state based on the apparent stability of 6_1 $C_6H_6\cdots Ar^1$. It is now believed from pulsed field ionization experiments that the dissociation energy has a upper limit 361 cm^{-1} in S_1 and therefore is ≤ 340 cm^{-1} in S_0.[27]

Since the first ab initio calculations for $C_6H_6\cdots Ar$ were performed by Hobza et al.,[28] there have been a number of such studies with increasing sophistication.[29−31] In the most recent work, Koch et al.[31] determined the ground state binding energy to be 389 ± 2 cm^{-1} and the excited state value to be 405 ± 2 cm^{-1}. The calculated difference in binding energies of 16 cm^{-1} is close to the experimental value of 21 cm^{-1}. The dissociation energies from the zero-point vibrational levels are 339 ± 2 cm^{-1} in the ground state and 355 ± 2 cm^{-1} in the excited state.[32] These values agree well with the experimental values of ≤ 340 and ≤ 361 cm^{-1}, respectively.[27] Koch et al. have recently reported a potential energy surface for the $C_6H_6\cdots Ar$ complex.[32] Throughout this paper the binding energies calculated by Koch et al. will be used.

The $C_6H_6\cdots Ar_2$ spectrum shows evidence for two isomers, one with the Ar atoms at equivalent positions on opposite sides of the ring (the so-called (1|1) structure; -41 cm^{-1} shift) and the other with both Ar atoms on the same side ((2|0) structure; -17 cm^{-1} shift).[33,34] In our experiments, the laser is tuned to excite the (1|1) isomer. Rotationally resolved spectra of the -41 cm^{-1} band proves it to be the 6^1_0 transition of $C_6H_6\cdots Ar_2$ (1|1), with the argon atoms located on the C_6 axis.[35] The benzene−argon distance in the ground electronic state was determined to be the same as that for $C_6H_6\cdots Ar$ within experimental error. The aromatic ring appears to effectively shield any interaction between the two argon atoms residing on opposite faces of the benzene molecule.

Our experiments on the dissociation of $(C_6H_6\cdots Ar)^+$ and $(C_6H_6\cdots Ar_2)^+$ monitor the $C_6H_6^+$ and $(C_6H_6\cdots Ar)^+$ products after dissociation, respectively. There are two possible pathways by which the product ions may be formed in the experiment. The first mechanism involves the complex sequentially absorbing two photons, being ionized and left in a vibrational state of the cation complex which subsequently dissociates. This is the process we wish to probe. The second mechanism is for the $(C_6H_6\cdots Ar_n)$ complex to dissociate on the S_1 surface after the absorption of one photon. Absorption of another photon by the $(C_6H_6\cdots Ar_{n-1})$ fragment will ionize it. If the second process is occurring it will interfere with our measurements.

The evidence from previous studies uniformly points to the second mechanism not occurring for $C_6H_6\cdots Ar$ and $C_6H_6\cdots Ar_2$ when exciting via 6^1. The evidence comes from a variety of sources: (i) early fluorescence studies of $C_6H_6\cdots Ar$ showed the complex to be a stable molecule in the 6^1 state[1]; (ii) a two-color REMPI study in which the van der Waals cation is prepared below its dissociation energy did not reveal any fragmentation when ionising through the 6^1 level;[33] (iii) the high-resolution spectrum recorded by Riedle et al. showed no broadening of the rotational lines in the 6^1_0 spectrum and, based on a model calculation, they suggest the lifetime is around 70 μs;[36] and (iv) molecular dynamics simulations show that dissociation from 6^1 is slow on a 10 ns time scale.[37] We conclude that with the <5 ns pulse width lasers used in our experiments, dissociation within S_1 is negligible for both $C_6H_6\cdots Ar$ and $C_6H_6\cdots Ar_2$ and the observed dissociation occurs wholly on the ionic surface.

The ionization potentials of $C_6H_6\cdots Ar$ and $C_6H_6\cdots Ar_2$ (1|1) have been determined to be $74\,383 \pm 2$ and $74\,221 \pm 2$ cm^{-1}, respectively, with shifts relative to the benzene ionization of -170 and -334 cm^{-1}, respectively.[33,38,39] The dissociation energy of the van der Waals ionic clusters, relative to the zero-point energy, can be calculated from a knowledge of the ground state dissociation energy of the neutral, the ionization potential of the parent van der Waals molecule, and the ionization potential of the fragment. For $(C_6H_6\cdots Ar)^+$, the value is determined to be 512 ± 3 cm^{-1}. The dissociation energy for the removal of one Ar atom in $(C_6H_6\cdots Ar_2$ $(1|1))^+$ is expected to be similar in value since, as discussed above, the argon atoms on opposite sides of the ring do not interfere with each other. From the ab initio calculations, scaled by the same value required to bring the ab initio and experimental values for $C_6H_6\cdots Ar$ dissociation into agreement, we estimate the dissociation energy of $C_6H_6\cdots Ar_2$ (1|1) to be 353 ± 2 cm^{-1}, giving a dissociation energy of $(C_6H_6\cdots Ar_2$ $(1|1))^+$ of 515 ± 4 cm^{-1}.[29] Within the uncertainties the values are the same for the two species and a value of 512 cm^{-1} is assumed for both.

The experimental evidence suggests that the $(C_6H_6\cdots Ar)^+$ complex dissociates rapidly above the dissociation energy.[27] The pulsed field ionization spectrum of $(C_6H_6\cdots Ar)^+$ shows no signal at the $(C_6H_6\cdots Ar)^+$ position above the ionic 4_1 level. Instead, at internal energies >629 cm^{-1} signal is seen at the benzene mass when the complex ion is excited.

3. Experimental Details

As this is the first paper from our group using the ion imaging−velocity mapping technique, we provide an overview of the apparatus and data acquisition procedure.

The experiment operates as follows. A pulsed supersonic expansion in the main chamber passes through a skimmer into the ionization region of a Wiley−McLaren[40] time-of-flight mass spectrometer (TOFMS). The molecular beam direction is along the axis of the TOFMS. A UV pulse from a frequency doubled dye laser, tuned to ionize the molecule of interest, produces cations and electrons in the center of the first acceleration region. The ions or electrons (depending on the mode of operation) are accelerated in two stages, travel along a field free region, and finally strike a position sensitive detector. The detector, consisting of an ion/electron amplifier and a phosphorescent screen, is gated on so that it is only activate when the species of interest arrives. A cooled CCD camera captures the image on the phosphor screen. The CCD image is downloaded to a computer which scans the image to determine the center pixel positions of the ions detected. These are stored as a histogram of ion counts versus position on the detector. The process continues as long as is required to obtain images with the desired signal-to-noise ratio.

The imaging apparatus utilizes the velocity mapping modification developed by Eppink and Parker.[18] The time-of-flight mass spectrometer is a Wiley−McLaren type with second-order space focus[41] to obtain high mass resolution with a short length flight tube (380 mm). When the spectrometer is operated in imaging mode the voltages have to be altered from those that are optimal for second-order space focusing. Simulations show that the mass resolution will be degraded slightly under these conditions; however, in the mass region of interest for the experiments presented here the resolution remains limited by the pulse duration of the laser (∼5 ns). A feature of velocity mapping is that the image is magnified. In our apparatus the magnification factor is ∼0.95. Calibration of the images was performed for each run by measuring the photoelectron image of benzene using the 6^0_1 transition as the resonant step.

The biggest influence on the mass resolution is the presence of molecules having different velocities parallel to the time-of-flight tube. In the dissociation experiments the effect of backward and forward recoils needs to be considered when determining the times at which the detector is gated on. The longer gating times needed for these experiments mean that the detector is active over a small range of masses centered at the mass of interest. This loss in resolution is not a problem in the series of experiments presented here since the other ions present are sufficiently different in mass to not be detected.

The time scale of dissociation to which our experiments are sensitive needs to be considered. For slow dissociation, where the ion travels some distance in the acceleration region before dissociating, the ion will be delayed due to the heavier mass in the initial accelerating region. The gate used for detection leads to ions with dissociation times >200 ns not being detected. We found by scanning the gate that for the $(C_6H_6\cdots Ar)^+$ and $(C_6H_6\cdots Ar_2)^+$ systems the dissociation occurred rapidly since the child ions arrived in a narrow time window.

The imaging apparatus has been used to record laser-induced photoelectron spectra to determine the vibrational distributions within the cations following ionization. For this work it was necessary to surround the entire time-of-flight tube with magnetic shielding (Co-Netic, Magnetic Shield Corp.).

The phosphor screen was viewed through a glass window on the end of the time-of-flight chamber using a video zoom lens (Navitar Zoom 7000) and captured on a CCD camera (Spectrasource Teleris 2).

We have used the technique of ion counting in measuring images. This technique has recently been introduced to imaging experiments, initially by Rogers et al.,[42] but subsequently reported independently and discussed in more detail by Chang et al.[43] A significant improvement in resolution is obtained using ion counting because the large area of each ion in an image is reduced to a single point (the central point of the spot produced by the ion).[43] In our experiments an image is accumulated on the CCD camera for five laser shots before being downloaded to the controlling computer. Unfortunately, with our camera the download time of an image (400 ms) prevented this process being performed on a shot-by-shot basis.

The laser system used in the experiments is a pulsed Nd:YAG laser (Continuum Surelite II) pumping a dye laser (Lambda Physik Scanmate 2E) fitted with a scanning doubling unit. A 10% beam splitter directs a small amount of the visible light to a pulsed wavemeter (Burleigh WA-4500). The UV output passes through a 1 mm iris before entering the vacuum chamber to ensure that the beam position remains constant. This is necessary as the image magnification is a function of the position of ionization along the time-of-flight axis. The laser beam is not focused onto the molecular beam. The polarization of the laser was set parallel to the detector face. Laser powers were kept low (∼0.5 μJ) to (i) prevent three-photon absorption by the complex,[27] (ii) minimize Coulombic repulsion between ions, and (iii) ensure that not too many ions appear in the center of the image, making ion counting impossible. Typically one ion is detected per laser shot.

The laser is tuned to the 6^1_0 transition of the species under investigation. Absorption of a second photon at this wavelength ionizes the complex. The vibrational distribution in the cations produced depends on the Frank−Condon factors for the transition from the S_1 state to the ionized species. Ions produced with vibrational energies in excess of the complex's dissociation energy fall apart. The child ions recoil and it is their velocity distribution that is measured. The wavelengths chosen for this study were 38 585 cm^{-1} for $C_6H_6\cdots Ar$ and 38 565 cm^{-1} for $C_6H_6\cdots Ar_2$. For $C_6H_6\cdots Ar$ the wavelength is the maximum of the 6^1_0 transition.[33] This is sufficiently removed from the $C_6H_6\cdots Ar_2$ (2|0) 6^1_0 transition to prevent interference by this species.[33] Absorption and ionization of $C_6H_6\cdots Ar_2$ (2|0) could lead to the loss of both argon atoms, forming bare benzene, the species detected in the experiment. For the $C_6H_6\cdots Ar_2$ case, we excite the (1|1) complex. The chosen wavelength is slightly red-shifted from the maximum of the $C_6H_6\cdots Ar_2$ (1|1) 6^1_0 transition to prevent absorption by $C_6H_6\cdots Ar_3$, which has its 6^1_0 transition blue-shifted from that of $C_6H_6\cdots Ar_2$.[33] This removes the possibility of the detected $C_6H_6\cdots Ar$ being formed by the removal of two argon atoms from $C_6H_6\cdots Ar_3$. While the 6^1_0 absorption transition of $C_6H_6\cdots Ar_2$ lies close to the corresponding transition in $(C_6H_6)_2$ (the 6^1_0 transition in $(C_6H_6)_2$ is split into two peaks centered at 38 567 cm^{-1} with a 4 cm^{-1} separation[41]), the dissociation products from this species (benzene cations) are not detected at the $C_6H_6\cdots Ar$ mass probed in the experiment.

Although care has been taken to remove interference from dissociating products, there remains a constant background in images. A problem with monitoring the benzene mass for the dissociation of $C_6H_6\cdots Ar$ is that the excitation wavelength is within the tail of the benzene 6^1_0 room temperature rotational contour. Residual benzene present within the chamber (from the previous expansion pulse) is observed as a very broad background. Fortunately, this interference is only weakly wavelength dependent since the room temperature benzene spectrum is quite broad and featureless in this region. Background data can thus be collected at wavelengths off-resonant with the complex absorption peaks. To ensure that backgrounds were reliable over the long time of data collection, the data were collected in two segments. Between the data runs, and at the end, an off-resonant background was recorded with the wavelength alternated between the high- and low-energy sides of the absorption peak (each was equidistant from the resonant wavelength). Because the absorption profile of room temperature benzene deviates slightly from linearity, the background required a small amount of scaling.

There is a sharp peak in the center of the images having the same shape as that of the molecular beam. We attribute this to off-resonance ionization or electron impact ionization of species in the molecular beam. (When the target species is ionized, the photoelectrons produced are accelerated parallel to the beam direction because of the electric field and can cause electron impact ionization of other species in the beam. We see, for example, Ar^+ produced via electron impact.) Because this peak is sharp, this part of the image has little influence on the resulting distributions and we simply ignore this region in the analysis.

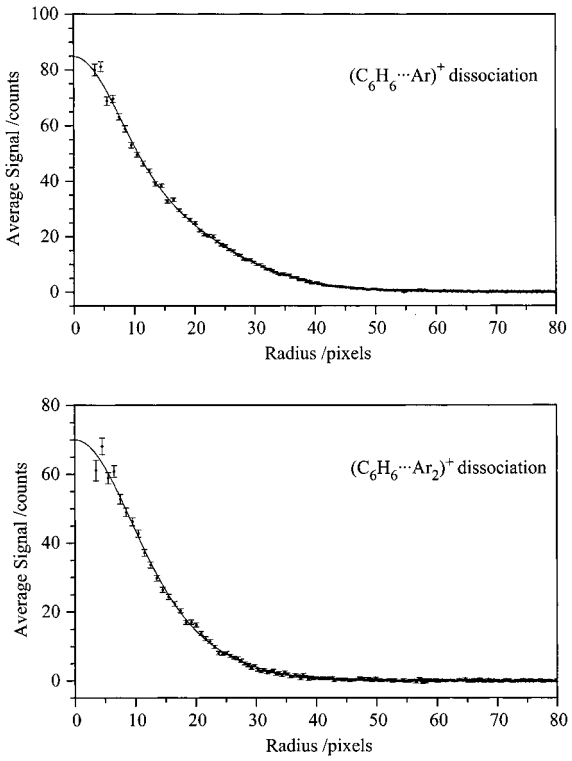

Figure 1. Radial plots extracted from the two-dimensional ion images for the $C_6H_6^+$ and $(C_6H_6\cdots Ar)^+$ fragments formed in the dissociation of $(C_6H_6\cdots Ar)^+$ and $(C_6H_6\cdots Ar_2)^+$, respectively. Error bars indicate ± 1 standard deviation as determined from the ion counting statistics. Solid curves are the sum of Gaussian fits to the data (see text).

Gas mixtures of 1% benzene (BDH 99.7%, freeze−pumped−thawed) in argon (BOC 99.997%) were prepared in a 6 L stainless steel pressure vessel to a total pressure of approximately 600 kPa. The output was regulated to the desired backing pressure (500 kPa in these experiments) as measured by a Bourdon gauge. The pulsed nozzle (General Valve Corp., 0.8 mm orifice) was situated 145 mm from the skimmer (Beam Dynamics, 1.5 mm orifice) while the distance between the nozzle and the interaction region is 200 mm.

4. Results and Data Analysis

If the complex dissociates on a time scale greater than its rotational period, the image will be circularly symmetric. The intensity profiles of slices through the images showed them to be so. Circular symmetry (i.e., $\beta = 0$) was also observed by Yoder et al. in their experiments on the dissociation of the pyrazine−argon van der Waals complex.[14] Because the images are circularly symmetric, the data can be analyzed by plotting the average intensity as a function of the distance from the center of the image, r, to create a so-called radial plot of the image. Radial plots of the images collected with the laser on and off resonance were subtracted to obtain the resulting dissociation radial plot. Radial plots are shown in Figure 1 for the $C_6H_6^+$ and $(C_6H_6\cdots Ar)^+$ fragments from the dissociation of $(C_6H_6\cdots Ar)^+$ and $(C_6H_6\cdots Ar_2)^+$, respectively.

Because the image is of a three-dimensional distribution projected onto a two-dimensional detector, the data have to be transformed (using an inverse Abel transform) to retrieve the original distribution.[17] The inverse Abel transform has been calculated in two complementary ways. The first method is similar to that given by Yoder et al., where the radial plots are first fitted to a sum of Gaussians.[14] In the current work, the sum of two Gaussians was found to be adequate to fit the radial plots. Fitting was performed using the Levenberg−Marquardt nonlinear least-squares fitting method.[45] The statistical nature of ion counting allows uncertainties to be easily determined (as the square root of the number of counts), and these were used as weights in the least-squares fit. Since the inverse Abel transform of a Gaussian is itself a Gaussian,[46] the three-dimensional radial distribution of the dissociating products can be calculated. For a sum of Gaussians given by

$$G(r) = \sum_i A_i e^{-k_i r^2}$$

the inverse Abel transform is given by

$$F(R) = \sum_i B_i e^{-k_i R^2} \qquad \text{where } B_i = A_i \sqrt{\frac{k_i}{\pi}}$$

The second method of data analysis is to perform the inverse Abel transform directly on the radial plot. For this we used the method of Hansen et al.[44] This method has the advantage that it can be used on arbitrary length data, and the data do not have to have constant spacing along the x-axis, although the method is simplified if this is the case. It was necessary to apply a three-point moving average to the data to get sufficiently smooth distribution curves since the inverse Abel transform is a differentiation process and any noise is amplified considerably.

After using either method to calculate the inverse Abel transform, it is then a simple matter of multiplying the radial intensity, $F(R)$, by R^2 to obtain the velocity population distribution. The velocity distribution is converted to an energy distribution by squaring the x-coordinate (which is in units of pixels at this stage), transforming from $(\text{pixels})^2$ to energy based on calibration data, and dividing the intensities by $E^{1/2}$ to correct the probabilities in the transformation from velocity space to energy space.[48] The experimental translational energy distribution describes the kinetic energy of the polyatomic fragment after dissociation. The total kinetic energy released is calculated from conservation of momentum and the resultant distribution normalized to give a probability distribution.

The distributions for the total kinetic energy released in the dissociation of each of the complexes are shown in Figure 2.

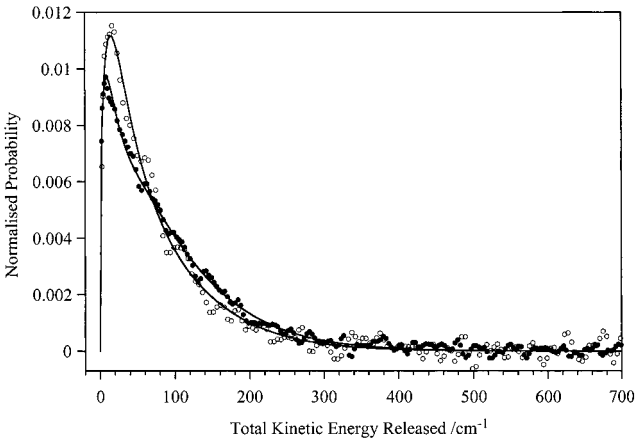

Figure 2. Distributions for the total kinetic energy released in the dissociation of $(C_6H_6\cdots Ar)^+$ and $(C_6H_6\cdots Ar_2)^+$ to form $C_6H_6^+$ and $(C_6H_6\cdots Ar)^+$, respectively. The solid lines come from the fitted Gaussian method of analysis while the points come from the direct inverse Abel transformation of the data. Filled circles are for $(C_6H_6\cdots Ar)^+$ dissociation while open circles are for $(C_6H_6\cdots Ar_2)^+$ dissociation.

TABLE 1: Parameters for the Total Kinetic Energy Released from the Dissociation of $(C_6H_6\cdots Ar)^+$ and $(C_6H_6\cdots Ar_2)^+$ Fitted to the Functional Form $P(E) = E^{1/2}\{c_1 \exp(-k_1E) + c_2 \exp(-k_2E)\}$, and the Average Kinetic Energy Released, $\langle\langle \Delta E\rangle\rangle$

van der Waals complex	fitted parameters				
	c_1	k_1/cm	c_2	k_2/cm	$\langle\langle \Delta E\rangle\rangle$/cm^{-1}
$C_6H_6\cdots Ar$	0.00384	0.0914	0.00176	0.0147	92 ± 4
$C_6H_6\cdots Ar_2$	0.00343	0.0482	0.00154	0.0154	78 ± 5

The solid lines come from the fitted Gaussian method of analysis while the points come from the direct inverse Abel transformation of the data. The distributions obtained by the two methods of analysis are identical within the experimental uncertainty. Although the total kinetic energy distributions from the two complexes look similar, there are subtle differences. The distribution from the dissociation of $(C_6H_6\cdots Ar_2)^+$ shows a slightly sharper rise and a faster decay compared with the $(C_6H_6\cdots Ar)^+$ distribution.

The transformation converting the radial plots of pixel intensity into the energy distribution, $P(E)$, transforms the original best fit sum of Gaussians of the radial plots into $P(E) = E^{1/2}\{c_1 \exp(-k_1E) + c_2 \exp(-k_2E)\}$. The parameters c_1, k_1, c_2, and k_2 for the two distributions are given in Table 1.

5. Discussion

5.1. Distribution of Cation Vibrational Energies Prior to Dissociation. Ideally, the experiment would measure the kinetic energy release distributions starting with a well-defined initial energy in the cation complex. However, in the photoionization process the cations are prepared in a range of vibrational energies depending on the Franck−Condon factors for transitions from the intermediate vibronic state. To relate the translational energy distributions of the fragments to the initial internal energies of the clusters it is necessary to know the distribution of ion energies formed in the photoionization of $C_6H_6\cdots Ar$ and $C_6H_6\cdots Ar_2$. The distribution of ion internal energies is mirrored in the photoelectron energy distribution, i.e., the photoelectron spectrum. Unfortunately, photoelectron spectra of these clusters are presently not available in the literature. Using the imaging apparatus we have attempted to measure the photoelectron spectra of $C_6H_6\cdots Ar$ and $C_6H_6\cdots Ar_2$ using REMPI via their 6^1_0 transitions but unfortunately the signal from the complexes could not be separated from that due to background, room-temperature benzene. With photoelectron data for the complexes unavailable, we have determined the initial vibrational distribution within the cluster cations based on the photoelectron spectrum of the benzene monomer.

Published photoelectron spectra,[49] which have been obtained using the time-of-flight technique, cannot be used to determine the cation vibrational population distribution because they do not extend over the full range of electron energies. Specifically, low-energy electrons are not seen and, since these electrons correspond with high internal energies in the cation, an accurate distribution of the vibrational levels above dissociation will not be forthcoming using these spectra. For this reason we have measured benzene REMPI photoelectron spectra afresh using the imaging apparatus, which is able to monitor the full range of electron energies. Full details will be published separately.[50]

The benzene photoelectron spectrum and that for the complexes can be related as follows. It is known that the presence of the Ar atom in aromatic−Ar van der Waals complexes generally has little effect on the vibrational levels of the aromatic.[1−4,7,36] For example, in the S_1 state of benzene rare-gas van der Waals clusters the observed frequencies remain unchanged from those in benzene with the exception of ν_{16}, which is seen to have a small shift.[1,36] The $C_6H_6^+$ vibrational frequencies are thus expected to be the same in the free and complexed ions, so the positions of bands in the photoelectron spectra will be the same (relative to the cation vibrational ground state) in $(C_6H_6\cdots Ar)^+$ and $(C_6H_6\cdots Ar_2)^+$ as in $C_6H_6^+$. The vibrational levels that have been observed in $(C_6H_6\cdots Ar)^+$ and $(C_6H_6\cdots Ar_2)^+$ confirm this.[39] Since the photoelectron intensities depend on the Franck−Condon factors, they will also be very similar for each of the three species. The benzene photoelectron spectrum therefore provides a good basis for determining the vibrational states populated after ionization of $C_6H_6\cdots Ar$ and $C_6H_6\cdots Ar_2$.

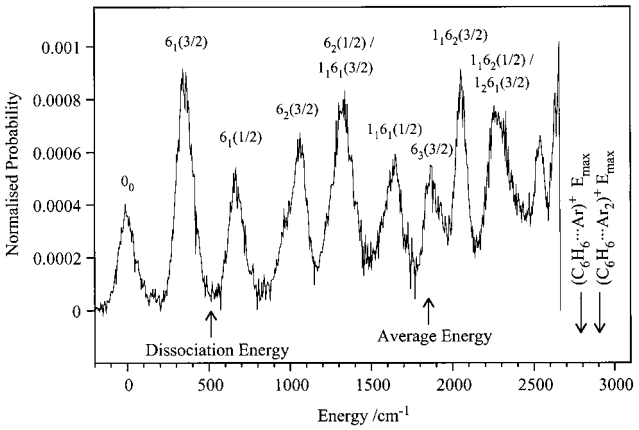

Figure 3. Distribution of population in the various vibrational states of the benzene cation as reflected in the photoelectron spectrum shown. The maximum energies for $(C_6H_6\cdots Ar)^+$ and $(C_6H_6\cdots Ar_2)^+$ prior to dissociation slightly exceed the range of the spectrum, as indicated. The diagram also indicates the dissociation energy for removal of a single Ar atom from each species and the average initial energies of those complexes formed with energy greater than the dissociation energy. For clarity, for the latter the average of the values for the two complexes (whose values differ by 60 cm^{-1}) is indicated.

The $C_6H_6^+$ vibrational population distribution is shown in Figure 3. The line widths seen in the figure are the result of the instrumental resolution. The dominant features have been assigned to vibrational levels within the cation based on the spectral assignments of Long et al.[49] The maximum internal energies available for the $(C_6H_6\cdots Ar)^+$ and $(C_6H_6\cdots Ar_2)^+$ cations are marked on the figure. With the change in the ionization potential and 6^1_0 transition frequency in the complexes, the maximum energy available to $(C_6H_6\cdots Ar)^+$ and $(C_6H_6\cdots Ar_2)^+$ after ionization is greater than that available to $C_6H_6^+$ by 124 and 246 cm^{-1}, respectively. Consequently, the 6^1_0 photoelectron spectrum for benzene does not extend to high enough energies to completely determine the high-energy end of the population distributions for the complexes. However, the missing section can be filled in by examining the photoelectron spectrum for REMPI via $6^1_0 1^1_0$ since the only change for this spectrum will be in the ν_1 progression intensities arising from the change in Franck−Condon factors.[49] The next peak in the $6^1_0 1^1_0$ photoelectron spectrum after 2663 cm^{-1}, the maximum excess energy in the 6^1_0 REMPI photoelectron spectrum of benzene, is at ~3010 cm^{-1}.[49,50] This is larger than the gaps outlined above, so no new peaks are expected in the $C_6H_6\cdots Ar$ and $C_6H_6\cdots Ar_2$ photoelectron spectra.

We assume that the distribution of population in the cation vibrational states for both $(C_6H_6\cdots Ar)^+$ and $(C_6H_6\cdots Ar_2)^+$ is the same as that for $C_6H_6^+$. By assuming that the background continues to increase linearly from 2663 cm^{-1} up to the

maximum available energy for each complex, the average energy above the dissociation energy, denoted $\langle E\rangle$, is estimated to be $\langle E\rangle \sim 1310$ cm^{-1} for $(C_6H_6\cdots Ar)^+$ and $\langle E\rangle \sim 1370$ cm^{-1} for $(C_6H_6\cdots Ar_2)^+$. The average internal energies are higher than these values by the dissociation energy (512 cm^{-1}).

$\langle E\rangle$ for $(C_6H_6\cdots Ar_2)^+$ is ~1370 cm^{-1}, well in excess of the dissociation energy of 512 cm^{-1} for loss of a second Ar atom. Since we observe the $(C_6H_6\cdots Ar)^+$ fragment after removal of a single argon atom from the $(C_6H_6\cdots Ar_2)^+$ parent, $(C_6H_6\cdots Ar_2)^+$ ions that are created with sufficient energy to allow removal of both argon atoms are not monitored in our experiment. A number of observations can be combined to deduce the $(C_6H_6\cdots Ar_2)^+$ internal energies that give rise to removal of a single argon atom. The pulsed field threshold ionization spectrum of $C_6H_6\cdots Ar$ shows no signal at the parent mass above the dissociation energy but signal is seen at the benzene mass, indicating that the $(C_6H_6\cdots Ar)^+$ van der Waals complex is not stable at energies above the dissociation energy.[27] Thus, after removal of an argon atom from $(C_6H_6\cdots Ar_2)^+$, further fragmentation will occur if the $(C_6H_6\cdots Ar)^+$ is formed in a vibrational level whose energy is greater than the $(C_6H_6\cdots Ar)^+$ dissociation energy. After REMPI of the 6^1_0 transition of $C_6H_6\cdots Ar_2$ we measure the $(C_6H_6\cdots Ar)^+$ signal to be only 0.66 that of $(C_6H_6\cdots Ar_2)^+$, consistent with the value of 0.7 seen by Weber and Neusser.[35] From the photoelectron spectrum (see Figure 3) we determine that ~15% of the $(C_6H_6\cdots Ar_2)^+$ ions are produced with energies less than the dissociation energy. These are the ions giving rise to the $(C_6H_6\cdots Ar_2)^+$ signal. In order to observe a $(C_6H_6\cdots Ar)^+$ signal that is two-thirds of the $(C_6H_6\cdots Ar_2)^+$ signal, only ~10% of the $(C_6H_6\cdots Ar_2)^+$ formed can produce a stable $(C_6H_6\cdots Ar)^+$ on dissociation. The remaining 75% of the $(C_6H_6\cdots Ar_2)^+$ ions therefore fragment completely into the three moieties.

The issue to be addressed is $\langle E\rangle$ for the $(C_6H_6\cdots Ar_2)^+$ that dissociate to form stable $(C_6H_6\cdots Ar)^+$, i.e., the ones the experiment is sensitive to. The $(C_6H_6\cdots Ar_2)^+$ ions whose dissociation we observe must have a minimum internal energy corresponding to the dissociation energy for loss of an Ar atom. The maximum energy these ions can possess can in principle be large, provided sufficient energy is removed as translation to leave the $(C_6H_6\cdots Ar)^+$ fragment with less than its dissociation energy (512 cm^{-1}). The experimental results show that the average translational energy released is only 79 cm^{-1} (see section 5.2 below). The maximum internal energy that a $(C_6H_6\cdots Ar_2)^+$ ion can have so that it releases 79 cm^{-1} into translation and is left with just insufficient energy to further fragment is ~(512 cm^{-1} × 2 + 79 cm^{-1} = 1103 cm^{-1}). $\langle E\rangle$ for the $(C_6H_6\cdots Ar_2)^+$ clusters between these bounds is ~350 cm^{-1}. This estimation is clearly indicative only. Nevertheless, it indicates the substantial reduction in the initial average energy available in the $(C_6H_6\cdots Ar_2)^+$ dissociation experiments compared with that in $(C_6H_6\cdots Ar)^+$ dissociation experiments, where the average initial energy above dissociation is ~1310 cm^{-1}.

5.2. Distribution of Translational Energy Released. A parameter for comparison between studies is the average energy transferred per collision, $\langle\Delta E\rangle$. For the dissociation of van der Waals molecules studied here, the ions prior to dissociation have a distribution of energies rather than a single value. Thus, we report a value for $\langle\langle\Delta E\rangle\rangle$, the average energy released averaged over all initial internal energies of the undissociated ion. The value of $\langle\langle\Delta E\rangle\rangle$ can easily be determined analytically from the parameters presented in Table 1 and is included in that table. For the dissociation of $(C_6H_6\cdots Ar)^+$ $\langle\langle\Delta E\rangle\rangle = 92 \pm 4$ cm^{-1} while for $(C_6H_6\cdots Ar_2)^+$ $\langle\langle\Delta E\rangle\rangle = 79 \pm 5$ cm^{-1}. We suggest the lower $\langle\langle\Delta E\rangle\rangle$ value obtained for the dissociation of $(C_6H_6\cdots Ar_2)^+$ is a direct consequence of the lower average energy in the $(C_6H_6\cdots Ar_2)^+$ cation before dissociation.

There are a number of very recent measurements of van der Waals dissociation recoil energy distributions by Yoder and Barker with which our values for the cation complexes can be compared.[15] These authors have measured the kinetic energy released during dissociation of a number of aromatic−X (where X = rare gas and small polyatomics) complexes from the triplet state. For dissociation within T_1 aromatic−Ar complexes, the average translational energy released is in the range 80−175 cm^{-1}. Our values for the two cation systems lie at the low end of this range and this may be associated with the low average internal energy prior to dissociation. The pyrimidine−Ar system, which has the lowest energy of the systems studied by Yoder and Barker (2543 cm^{-1} initial energy), has an average energy of 89 cm^{-1}, quite close to the values measured here.

The similarity in behavior for the neutral, albeit excited state triplet, and charged radical species is interesting. Yoder and Barker note the similarity in the distributions they obtain for a variety of aromatics with a wide range of initial energies. They postulate that this similarity may arise from the involvement of the low-frequency out-of-plane mode ν_{16} in the dissociation. The same effect may be responsible for the similarity between our results for the benzene−Ar_n cation and those seen for these neutral systems.

The overall shape of the distributions we obtain can be compared with those obtained by Yoder and Barker, which are shown in Figure 5 of their paper. We find that the $(C_6H_6\cdots Ar)^+$ and $(C_6H_6\cdots Ar_2)^+$ distributions are very similar in overall shape to those reported by Yoder and Barker although the distributions for cation dissociation are generally narrower. A particular aspect of our cation distributions and the distributions for triplet state aromatics reported by Yoder and Barker is the lack of a high ΔE tail in both. This is in contrast to the results of an earlier report by Yoder et al. who studied the translational energy released during dissociation of T_1 pyrazine−Ar using ion imaging.[14] These authors report a long tail to the distribution, with the probability not decaying to 10^{-4} until $\Delta E \sim 740$ cm^{-1}. In Yoder and Barker's time-of-flight study the pyrazine−Ar distribution does not have this long tail and decays to 10^{-4} at $\Delta E \sim 425$ cm^{-1}. In comparison, the $(C_6H_6\cdots Ar)^+$ distribution decays to 10^{-4} at $\Delta E \sim 400$ cm^{-1}, while the $(C_6H_6\cdots Ar_2)^+$ distribution decays to 10^{-4} at $\Delta E \sim 370$ cm^{-1}.

It is not clear at this juncture whether the different shapes for the large ΔE segment of the T_1 pyrazine−Ar distribution reflect differences in the sensitivity of the two experimental techniques, ion imaging and time-of-flight, to this part of the distribution. Interestingly, our measurements utilize ion imaging and we do not observe a long tail in the distributions. The high-energy tail seen by Yoder et al. in their ion imaging study is within the average energy available to the $(C_6H_6\cdots Ar)^+$ complex. Thus, on energetic grounds there is the opportunity for the $(C_6H_6\cdots Ar)^+$ cluster to show a high ΔE tail.

Recent quasiclassical trajectory simulations reproduce the experimental translational energy distributions for pyrazine−Ar and methylpyrazine−Ar van der Waals complex dissociation quite well.[51] The calculated distributions suggest more transfer in the high translational energy tail than does the experimental data of Yoder and Barker.[15] Importantly, the calculations reproduce the experimental trend for there to be only a small fraction of the energy transferred to translation in the dissociation process (see section 5.3 below).

In this context, it is interesting to note that the quasiclassical trajectory calculations on the benzene−argon system performed by Bernshtein and Oref predict a high ΔE tail in the distribution.[21] These calculations were undertaken at an internal energy of 51 900 cm^{-1}. The tail is more significant for the Lennard-Jones potential than for the ab initio potential. These quasiclassical trajectory calculations showed the average kinetic energy released from the dissociation process to be 150 and 43 cm^{-1} for the Lennard-Jones and ab initio potentials, respectively. Based on our results and those for the T_1 aromatic−Ar systems by Yoder and Barker, the latter figure appears to be lower than expected by a factor of 2 or more.

Yoder et al. have shown that statistical modeling of the translational energy released distribution function leads to an overestimation of the recoil energy.[14] Since our distributions are narrower than theirs, such calculations will be similarly inaccurate in our case. Accurate modeling of these systems requires a more sophisticated treatment, as shown by the recent trajectory calculations.[51]

5.3. Residual Internal Energy in the Polyatomic Fragments. The kinetic energy distributions for dissociation of both van der Waals cation species show probabilities that peak at very low energy (10−15 cm^{-1}) and decay such that the probability of releasing kinetic energies above 400 cm^{-1} is very small. For $(C_6H_6\cdots Ar)^+$, 400 cm^{-1} represents $\sim 1/6$ of the maximum energy available and $\sim 1/3$ of the average energy available. Thus, in this case the $C_6H_6^+$ fragments must contain significant vibrational and/or rotational energy. We have discussed in section 5.1 that for dissociation of $(C_6H_6\cdots Ar_2)^+$ the residual energy in the $(C_6H_6\cdots Ar)^+$ fragment is sufficient in 75% of cases for it to further fragment to $C_6H_6^+$.

This behavior whereby only a small amount of the available energy is released into kinetic energy of the fragments appears to be a common feature of the van der Waals dissociations where kinetic energy release has been observed. It is a feature of all of the T_1 aromatic−X complexes studied by Yoder and Barker,[15] in which the initial energy ranged up to ∼8000 cm^{-1}. Dissociation of ethylene dimers in the ground electronic state shows a similar trend.[52] The average kinetic energy released in ethylene and deuterated ethylene dimer dissociation following excitation to ∼800 cm^{-1} above the dissociation energy is only 71 cm^{-1}. For dissociation of $(C_2H_4)_2$, the loss of 71 cm^{-1} into translation means that only the ground vibrational state can be populated and all of the remaining energy (i.e., ∼730 cm^{-1}) is taken up as rotational energy of the fragments.

The partitioning of considerable amounts of energy into rotation is also observed in the dissociation of *s*-tetrazine−argon,[3] pyrimidine dimers,[53] and *p*-difluorobenzene−argon.[10] It appears from the evidence available that not only is it generally the case that only a small fraction of the available energy is released as kinetic energy of the fragments, but it also appears that significant rotational excitation of the fragments accompanies the dissociation.

The data available for the $(C_6H_6\cdots Ar_2)^+$ and $(C_6H_6\cdots Ar_2)^+$ dissociations do not allow us to comment definitively on the partitioning of energy within the polyatomic fragment's rotational and vibrational degrees of freedom. We are currently undertaking experiments to pursue the issue of the partitioning of energy in van der Waals dissociation.

The results of our experiment and those mentioned above can be explained qualitatively by the momentum gap law introduced by Ewing.[54] This theory predicts that van der Waals dissociation will populate states that consist of low changes in momentum (i.e., consist of low kinetic energy releases). The basis of this law comes from the poor overlap of the van der Waals molecule wave function and the translational wave functions of the separating species.

5.4. Comparison with Energy Transfer Experiments. We noted in the Introduction that the van der Waals dissociation experiments are related to collision-induced energy transfer. In addition to the obvious difference in collision energy between van der Waals molecule dissociation and collision-induced vibrational energy transfer, the former having zero collision energy, it has been pointed out by a number of authors that van der Waals molecule dissociation is also far more constrained.[14,15,21] This is because it always starts from the same geometry while a collision can take place anywhere around the molecule. While the two types of "collisions" have the same interaction potential, in van der Waals molecule dissociations only a portion of the potential is sampled. It is thus interesting to compare the trends seen in our study of half-collisions with the behavior seen in full collisions.

Unfortunately, no experimental data exist for collisional energy transfer involving benzene cations and Ar with which our data can be compared. However, in order to illustrate how the translational distributions measured in van der Waals dissociation experiments can be related to collisional energy transfer experiments, we compare our results with studies of energy transfer in benzene−Ar collisions.

Energy transfer experiments have been performed at room temperature on highly excited ground state benzene using a variety of collision partners.[55−57] A major difference between room temperature energy transfer and van der Waals complex dissociation is that the former involves both "up" and "down" collisions while the latter involves only "down"transfer. The two results can be compared by assuming the translational energy distribution from the $(C_6H_6\cdots Ar)^+$ van der Waals cation dissociation matches the downward energy transfer probability function for benzene−Ar collisions. The upward distribution can be constructed at a particular vibrational energy and temperature from microscopic reversibility.[58] The up and down distributions can then be combined to determine a value for the average energy transferred per collision at that energy and temperature. Using this approach we estimate that at a vibrational energy ∼2000 cm^{-1} in S_0 benzene, a similar amount of energy to that used in our current work, the average energy transferred per collision is ∼10 cm^{-1}. Extrapolation of the experimental energy transfer data shows that at an average internal energy of 2000 cm^{-1} the average energy transferred per collision is a few (∼2−3) wavenumbers.

6. Conclusion

Ion imaging has been used to measure the recoil velocities of the polyatomic fragments following dissociation of the van der Waals cation complexes $(C_6H_6\cdots Ar_2)^+$ and $(C_6H_6\cdots Ar)^+$ by ejection of an argon atom. The ions were produced by photoionization of the neutral clusters via the 6^1_0 intermediate state, which leads to a range of initial vibrational energies in the cation prior to dissociation. Since no photoelectron spectra exist for the benzene−argon van der Waals clusters, and only an incomplete photoelectron spectrum was available in the literature for benzene,[49] the photoelectron spectrum of benzene has been measured to determine the initial vibrational distribution. On the basis of the observed spectroscopic behavior of aromatic−argon complexes, we assume the initial distribution for the cation complexes will be the same as that observed for the benzene cation. In the case of $(C_6H_6\cdots Ar_2)^+$ we observe only the small fraction of the clusters that dissociate to form $(C_6H_6\cdots Ar)^+$ below its dissociation energy. The average

energies above the dissociation energy prior to fragmentation were determined to be ~1310 cm^{-1} for $(C_6H_6\cdots Ar)^+$ and 350 cm^{-1} for $(C_6H_6\cdots Ar_2)^+$.

The average energies released in the dissociation of $(C_6H_6\cdots Ar)^+$ and $(C_6H_6\cdots Ar_2)^+$ were 92 ± 4 and 79 ± 5 cm^{-1}, respectively. This indicates that a majority of the energy remains as internal energy (i.e., in vibrational and/or rotational energy) of the polyatomic fragment. This effect has been seen previously in a number of other studies of van der Waals molecule dissociation. The values for the average energy released are similar to those obtained in other studies involving aromatic van der Waals molecules.

Although the energy distributions are qualitatively similar, they have discernible differences which we attribute to the differences in the average initial energies of the dissociating complexes.

Acknowledgment. This work was undertaken with the financial support of the Australian Research Council and Flinders University. The authors express their gratitude to the staff the School of Chemistry, Physics and Earth Sciences Engineering and Electronic Workshops for their technical support. J.R.G. thanks the Ferry Foundation for the award of a Research Scholarship.

References and Notes

(1) Stephenson, T. A.; Rice, S. A. *J. Chem. Phys.* **1984**, ***81***, 1083.
(2) Jacobson, A.; Humphrey, S.; Rice, S. A *J. Chem. Phys.* **1988**, *89*, 5624.
(3) Brumbaugh, D. V.; Kenny, J. E.; Levy, D. H. *J. Chem. Phys.* **1983**, *78*, 3415.
(4) Gilbert, B. D.; Parmenter, C. S.; Su, M.-C.; Oh, H.-K.; Zhao, Z.-Q. *Appl. Phys. B* **1994**, *59*, 397.
(5) Nimlos, M. R.; Young, M. A.; Bernstein, E. R.; Kelley, D. F. *J. Chem. Phys.* **1989**, *91*, 5268.
(6) Becucci, M.; Lakin, N. K.; Pietraperzia, G.; Castelluci, E.; Brechignac, P.; Coutant, B.; Hermine, P. *J. Chem. Phys.* **1999**, *110*, 9961.
(7) Gilbert, B. D.; Parmenter, C. S.; Oh, H.-K. *J. Phys. Chem.* **1995**, *99*, 2444.
(8) Hineman, M. F.; Kim, S. K.; Bernstein, E. R.; Kelly, D. F. *J. Chem. Phys.* **1992**, *96*, 4904.
(9) Zhang, X.; Smith, J. M.; Knee, J. L. *J. Chem. Phys.* **1992**, *97*, 2943.
(10) Lembach, G.; Brutschy, B. *J. Phys. Chem. A* **1998**, *102*, 6068.
(11) Nishiyama, I.; Hanazaki, I. *Chem. Phys. Lett.* **1985**, *117*, 99.
(12) Vernon, M. F.; Lisy, J. M.; Kwok, H. S.; Krajnovich, D. J.; Tramer, A.; Shen, Y. R.; Lee, Y. T. *J. Phys. Chem.* **1981**, *85*, 3327.
(13) Johnson, R. D.; Burdenski, S.; Hoffbauer, M. A.; Giese, C. F.; Gentry, W. R. *J. Chem. Phys.* **1986**, *84*, 2624.
(14) Yoder, L. M.; Barker, J. R.; Lorenz, K. T.; Chandler, D. W. *Chem. Phys. Lett.* **1999**, *302*, 602.
(15) Yoder, L. M.; Barker, J. R. *Phys. Chem. Chem. Phys*. **2000**, *2*, 813.
(16) Chandler, D. W.; Houston, P. L. *J. Chem. Phys*. **1987**, *87*, 1445.
(17) Heck, A. J. R.; Chandler, D. W. *Annu. Rev. Phys. Chem.* **1995**, *46*, 335.
(18) Eppink, A. T. J. B.; Parker, D. H. *Rev. Sci. Instrum.* **1997**, *68*, 3477.
(19) Chandler, D. W.; Parker, D. H. In *Advances in photochemistry*; Neckers, D. C., Volman, D. H., von Bünau, G., Eds.; Wiley-Interscience: New York, 1999; Vol. 25, p 59.
(20) Rice, S. A. *J. Phys. Chem.* **1986**, *90*, 3063.
(21) Bernshtein, V.; Oref, I. *Chem. Phys. Lett.* **1999**, *300*, 104.
(22) Knight, A. E. W.; Parmenter, C. S.; Schuyler, M. W. *J. Am. Chem. Soc.* **1975**, *97*, 1993.
(23) Stephenson, T. A.; Radloff, P. A.; Rice, S. A. *J. Chem. Phys.* **1983**, *81*, 1060.
(24) Nicholson, J. A.; Lawrance, W. D.; Fischer, G. *Chem. Phys.* **1995**, *196*, 327.
(25) Menapace, J. A.; Bernstein, E. R. *J. Phys. Chem.* **1987**, *91*, 2533.
(26) Weber, Th.; von Bargen, A.; Riedle, E.; Neusser, H. J. *J. Chem. Phys.* **1990**, *92*, 90.
(27) Krause, H.; Neusser, H. J. *J. Chem. Phys.* **1993**, *99*, 6278.
(28) Hobza, P.; Selzle, H. L.; Schlag, E. W. *J. Chem. Phys.* **1991**, *95*, 391.
(29) Hobza, P.; Bludsk, O.; Selzle, H. L.; Schlag, E. W. *Chem. Phys. Lett.* **1996**, *250*, 402.
(30) Klopper, W.; Lüthi, H. P.; Brupbacher, Th.; Bauder, A. *J. Chem. Phys.* **1994**, *101*, 9747.
(31) Koch, H.; Fernández, B.; Christiansen, O. *J. Chem. Phys.* **1998**, *108*, 2784.
(32) Koch, H.; Fernández, B.; Makarewicz, J. *J. Chem. Phys.* **1999**, *111*, 198.
(33) Schmidt, M.; Mons, M.; Le Calvé, J. *Chem. Phys. Lett.* **1991**, *177*, 371.
(34) Scherzer, W.; Selzle, H. L.; Schlag, E. W. *Chem. Phys. Lett.* **1992**, *195*, 11.
(35) Weber, Th.; Neusser, H. J. *J. Chem. Phys.* **1991**, *94*, 7689.
(36) Riedle, E.; Sussmann, R.; Webber, Th.; Neusser, H. J. *J. Chem. Phys.* **1996**, *104*, 865.
(37) Vacek, J.; Hobza, P.; Jortner, J. *J. Phys. Chem. A* **1998**, *102*, 8268.
(38) Chewter, L.; Müller-Dethlefs, K.; Schlag, E. W. *Chem. Phys. Lett.* **1987**, *135*, 219.
(39) Neusser, H. J.; Krause, H. *Chem. Rev.* **1994**, *94*, 1829.
(40) Wiley: W. C.; McLaren, I. H. *Rev. Sci. Instrum.* **1955**, *26*, 1150.
(41) Boesl, U.; Weinkauf, R.; Schlag, E. W. *Int. J. Mass Spectrom. Ion Processes* **1992**, *112*, 121.
(42) Rogers, L. J.; Ashfold, M. N. R.; Matsumi, Y.; Kawasaki, M.; Whitaker, B. J. *Chem. Phys. Lett.* **1996**, *258*, 159.
(43) Chang, B.-Y.; Hoetzlein, R. C.; Mueller, J. A.; Geiser, J. D.; Houston, P. L. *Rev. Sci. Instrum.* **1998**, *69*, 1665.
(44) Hopkins, J. B.; Powers, D. E.; Smalley, R. E. *J. Phys. Chem.* **1981**, *85*, 3739.
(45) Press: W. H.; Teukolsky, S. A.; Vetterling, W. T.; Flannery, B. P. *Numerical Recipes in FORTRAN*; Cambridge University Press: Cambridge, UK, 1992.
(46) Bracewell, R. N. *The Fourier Transform and Its Applications*, 2nd ed.; McGraw-Hill: New York, 1977.
(47) Hansen, E. W.; Law, P.-L. *J. Opt. Soc. Am. A* **1985**, *2*, 510.
(48) Bromse, D. S.; Cross, J. B.; Valentini, J. J. *J. Chem. Phys.* **1983**, *78*, 7175.
(49) Long, S. R.; Meek, J. T.; Reilly, J. P. *J. Chem. Phys*. **1983**, *79*, 3206.
(50) Gascooke, J. R.; Lawrance, W. D., manuscript in preparation.
(51) Yoder, L. M.; Barker, J. R. *J. Phys. Chem. A*, in press.
(52) Hoffbauer, M. A.; Liu, K.; Giese, C. F.; Gentry, W. R. *J. Chem. Phys.* **1983**, *78*, 5567.
(53) Saigusa, H.; Forch, B. E.; Chen, K. T.; Lim, E. C. *Chem. Phys. Lett.* **1983**, *101*, 6.
(54) Ewing, G. E. *J. Chem. Phys.* **1979**, *71*, 3143.
(55) Yerram, M. L.; Brenner, J. D.; King, K. D.; Barker, J. R. *J. Phys. Chem.* **1990**, *94*, 6341.
(56) Barker, J. R.; Toselli, B. M. *Int. Rev. Phys. Chem.* **1993**, *12*, 305.
(57) Barker, J. R.; Brenner, J. D.; Toselli, B. M. In *Vibrational Energy Transfer Involving Large and Small Molecules*; Adv. Chem. Kinet. Dyn., Vol. 2; Barker, J. R., Ed.; JAI Press: Greenwich, CT, 1995; p 393.
(58) Gilbert, R. G.; Smith, S. *Theory of Unimolecular and recombination reactions*; Blackwell Scientific Publications: London, 1990.